Research Article

Dynamic Response of Pile-Raft Systems with Various Forms of Connection under Cyclic Condition

Juan Du, Xiao-Peng Lei, Di-Fan Ren, Zai-Cheng Wang, and Yang Zhang 📍

School of Civil Engineering and Architecture, Hainan University, Haikou 570228, China

Correspondence should be addressed to Yang Zhang; a314261366@163.com

This study aimed to examine the aseismic performance of the pile-raft systems with various connection forms. The related shaking table test and numerical simulation were performed for in-depth investigation. The acceleration response spectra on the top of the soil layer and raft were obtained and plotted for contrastive analysis based on the model test at a reduced scale of 1 : 30 and finite element numerical simulation. Accordingly, the working mechanisms of the pile-raft systems in conventional connections with the embedment of the compressible blocks and cushion layers under cyclic loading were explored. The results showed that the embedment of the cushion layer on the pile top could most significantly mobilize the potential of the foundation soil, effectively reduce the bending moment peak of the pile, and reduce the acceleration amplification effect on the top of the soil layer and raft. The embedment of the compressible block on the pile top most markedly reduced the bending moment peak of the pile and effectively mobilized the potential of the foundation soil, which was most favorable for lowering the amplification effect of acceleration on the top of the soil layer and raft.

1. Introduction

Pile raft foundations (PRFs) have been extensively used in many engineering practices owing to a series of advantages including favorable seismic performance, slight settlement, and high bearing capacity [1–4]. Piles in PRF are generally utilized as settlement reducers, not structural members for carrying load. In design, fewer piles may be installed to meet the settlement requirements, but result in higher axial stress in the piles. In addition, the rigid connection between the pile head and raft will produce large shear stresses and bending moments at the connection point, especially under seismic loads. Therefore, the shear and bending failure on the pile head may precede the soil failure [5].

To address the high stress problems of piles and rafts [6, 7], Wong et al., Lawal, and Doi et al. [8–10] proposed disconnected pile-raft systems, which settled an interposed layer between the raft and piles. According to the materials used in the interposed layer, disconnected pile-raft systems can be divided into cushion layer pile-raft systems (CLPRS) and compressible block pile-raft systems (CBPRS).

Laboratory tests and numerical simulations revealed that the settlement and bending moments in the piles and rafts of CLPRS were effectively dropped under static load conditions [11, 12]. This was attributed to the cushion layer effectively regulating the bearing capacity of the foundation, playing an important role in improving the load transfer mechanism of the pile and reducing the overall settlement and stiffness of the foundation [13–15]. As for CBPRS, researches have dedicated that the appropriate stiffness of compressible blocks can be selected to adjust the reaction force distribution at the pile head and obtain the specified settlement [16, 17].

The mechanism of pile-raft systems under seismic conditions is relatively less studied compared with that under static load conditions, mainly focusing on the PRF and CLPRS. In general, the interaction and acceleration of the pile-raft systems are affected under seismic conditions. Kumar et al. [18] conducted a series of centrifuge model tests to evaluate the behavior of PRF under dynamic loading conditions and found that the maximum displacement and bending moment were observed at the pile head, which was

attributable to the rigid fixity of the piles with the raft. The crossover point in the bending moment profile was observed at shallow depths for all cases of loading. Fioravante and Giretti [19] used a series of centrifuge model tests to investigate the load transfer mechanisms of PRF and CLPRS and found that PRF acted as a settlement reducer while CLPRS played the role of soil reinforcement. Based on the shaking table tests, Azizkandi et al. [20, 21] found that PRF and CLPRS effectively reduced the ground settlements. It was also concluded that CLPRS decreased the maximum bending moment of piles by 20%–60%, based on input motion amplitudes and cushion layer material. Han et al. [22] used numerical simulation on the difference in the seismic responses of PRF and CLPRS and found that the seismic absorption effect of a cushion was good, with an absorption ratio of approximately 0.85.

While it has been confirmed that CLPRS have some good seismic performance under seismic conditions, the dynamic behavior of CBPRS, such as bending moments in the piles and ground motion effect, has not been reported experimentally or numerically.

In this study, a series of model tests on the pile-raft systems with various connection modes was conducted to further examine the operating mechanism of the pile-raft systems under dynamic loading conditions. Additionally, finite element software was used for numerical simulations and supplementary analysis of the model tests. The pile-soil interaction, the bending moment of the pile, and the acceleration of the soil and raft of PRF, CLPRS, and CBPRS were analyzed to elaborate on the dynamic performance of the pile-raft systems.

2. Shaking Table Test Set-Up

2.1. Testing Apparatus.
All the experiments in the present study were carried out using the shaking table at Hainan University, as shown in Figure 1. The shaking table had a maximum vibration acceleration of 3 g, maximum horizontal displacement along the shaking direction of ±7 mm, and a vibration frequency of 1–3000 Hz. The rubber membrane was applied inside the model box, which could effectively weaken the reflection and scattering effects of dynamic waves on the boundary.

2.2. Model Configuration.
High acceleration and a scaled model were adopted in the shaking table tests to simulate the same stress conditions in the prototype. Based on the characteristics of the model and the performances of the shaking table, Young's modulus (E), length (L), and density (ρ) were selected as basic physical quantities to acquire the similarity ratio. For example, a prototype pile-raft modulus of 3×10^4 MPa was modeled by 3×10^3 MPa in shaking table tests; a prototype pile length of 7.5 m was modeled by 0.25 m; and a prototype pile-raft density of 2.36×10^3 kg/cm^3 was modeled by 1.18×10^3 kg/cm^3. Furthermore, the similarity ratios of other physical model parameters, such as time (t) and acceleration (a), were deduced from the Buckingham π theorem [23]. The similarity ratios of the model system are shown in Table 1. The properties of elements used in the pile-raft systems are shown in Table 2. Three types of the pile-raft systems are shown in Figure 2.

2.3. Soil Sample.
The model ground used in the test was natural organic matter-disseminated sand (OMDS) on Hainan Island. Hainan Island is located at the edge of the Circum-Pacific Seismic Belt, with a great earthquake intensity in the northern region [24]. In addition, the partial regions are characterized by the extensive distribution of a large amount of OMDS [25]. Its basic engineering properties acquired using geotechnical tests and consolidated drained triaxial tests, which are concluded in the Chinese Standard for geotechnical testing method [26], are shown in Table 3. The soil was packed layer by layer to ensure the uniformity of the soil in the model box. The soil was divided into six layers; each layer was 60 mm, and the total height was 300 mm. The surface of each layer was scraped to ensure good contact between the layers filled separately.

2.4. Instrumentation.
Figure 3 displays the placement of instruments. Six electrical resistance-type strain gauges, three pore water pressure sensors, and three soil pressure sensors were arranged 5 cm, 12.5 cm, and 20 cm away from the top of the pile. The strain gauges were symmetrically distributed on both sides of the pile along the shaking direction. A soil pressure sensor was also set at the corresponding height with each pair of strain gauges. The accelerometers were set on the shaking table, the top of the raft, and the surface of the soil.

The pore water pressure sensor [27] used is the DSP-I-3BS high-precision miniature split-type pore pressure sensor produced by the Institute of Engineering Mechanics, China Earthquake Administration, to measure the time characteristics of the excess pore pressure under vibration.

The strain gauge used is the BFH120-10AA-D150 strain gauge produced by Guangce Electronics Co., Ltd. in Heshan District, Yiyang City. It has a rated resistance of 120 Ω and a sensitivity factor of 2.0 ± 1%. It is symmetrically attached to both sides of the pile body along the vibration direction to measure the strain of the pile body.

The accelerometer selected is the piezoelectric accelerometer produced by Beijing Spectrum Century Technology Development Co., Ltd. It is placed on the vibration table, top of the soil, and top of the raft to obtain the acceleration time history curves of the vibration table input, soil surface, and raft top.

The dynamic acquisition system adopts the IMC dynamic data acquisition instrument from Germany, as shown in Figure 1. It has 16 channels and is connected to the soil pressure box and pore pressure sensor through the bridge box to obtain the corresponding signals, which are ultimately converted into
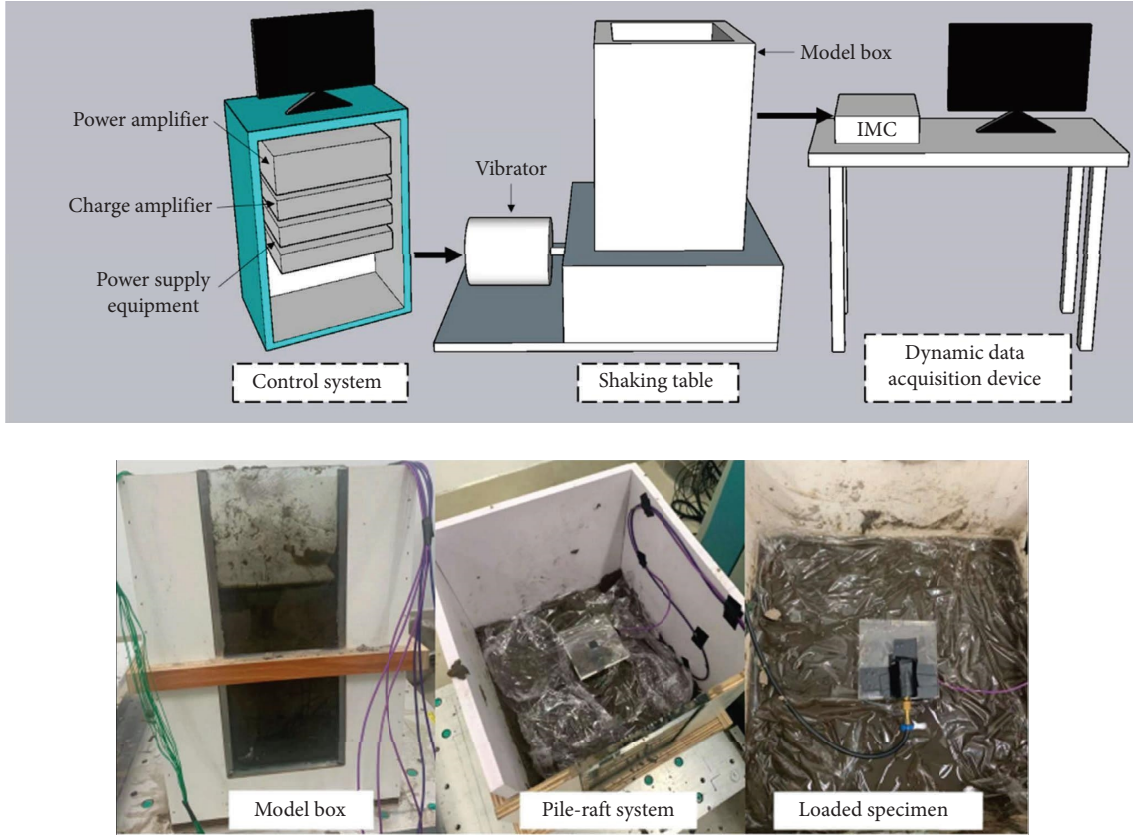
FIGURE 1: Schematic drawing of the shaking table test system.

TABLE 1: Similarity ratio of the model system.

Physical quantity	Similitude relation*	Adopted similarity ratio
Young's modulus, E	$S_E = E_m/E_p$	1/10
Density, ρ	$S_\rho = \rho_m/\rho_p$	1/2
Length, L	$S_l = L_m/L_p$	1/30
Time/natural period, t	$S_t = S_l\sqrt{S_\rho/S_E}$	0.0745
Acceleration, a	$S_a = S_E/(S_p \times S_l)$	6

*S refers to the ratio of the model to the prototype, m in the subscript refers to the model, and p refers to the prototype.

TABLE 2: Properties of the elements.

Element	Material	Prototype (mm)	Model (mm)	Young's modulus (MPa)	Poison ratio
Raft	Organic glass	$1800 \times 1800 \times 300$	$60 \times 60 \times 10$	3000	0.2
Pile	Organic glass	$300 \times 300 \times 7500$	$10 \times 10 \times 250$	3000	0.2
Compressible block	Cork	$300 \times 300 \times 300$	$10 \times 10 \times 10$	0.12	0.25
Cushion layer	Rubber	$1800 \times 1800 \times 300$	$60 \times 60 \times 10$	2000	0.25
Raft	Organic glass	$1800 \times 1800 \times 300$	$60 \times 60 \times 10$	3000	0.2

electrical signals. The accelerometer acquisition device uses the WS-5921/U60216-DA1 vibration table control and signal acquisition device inside the shaking table, with 8 channels, directly connected to the accelerometer sensor through a wire, and outputs acceleration values.

2.5. *Test Program.* A sine wave with an acceleration of 1.8 g was adopted to scale the peak ground acceleration of 0.3 g so as to examine the effect of the earthquake intensity of the northern region on Hainan Island. In combination with the test conditions, the test samples were divided into
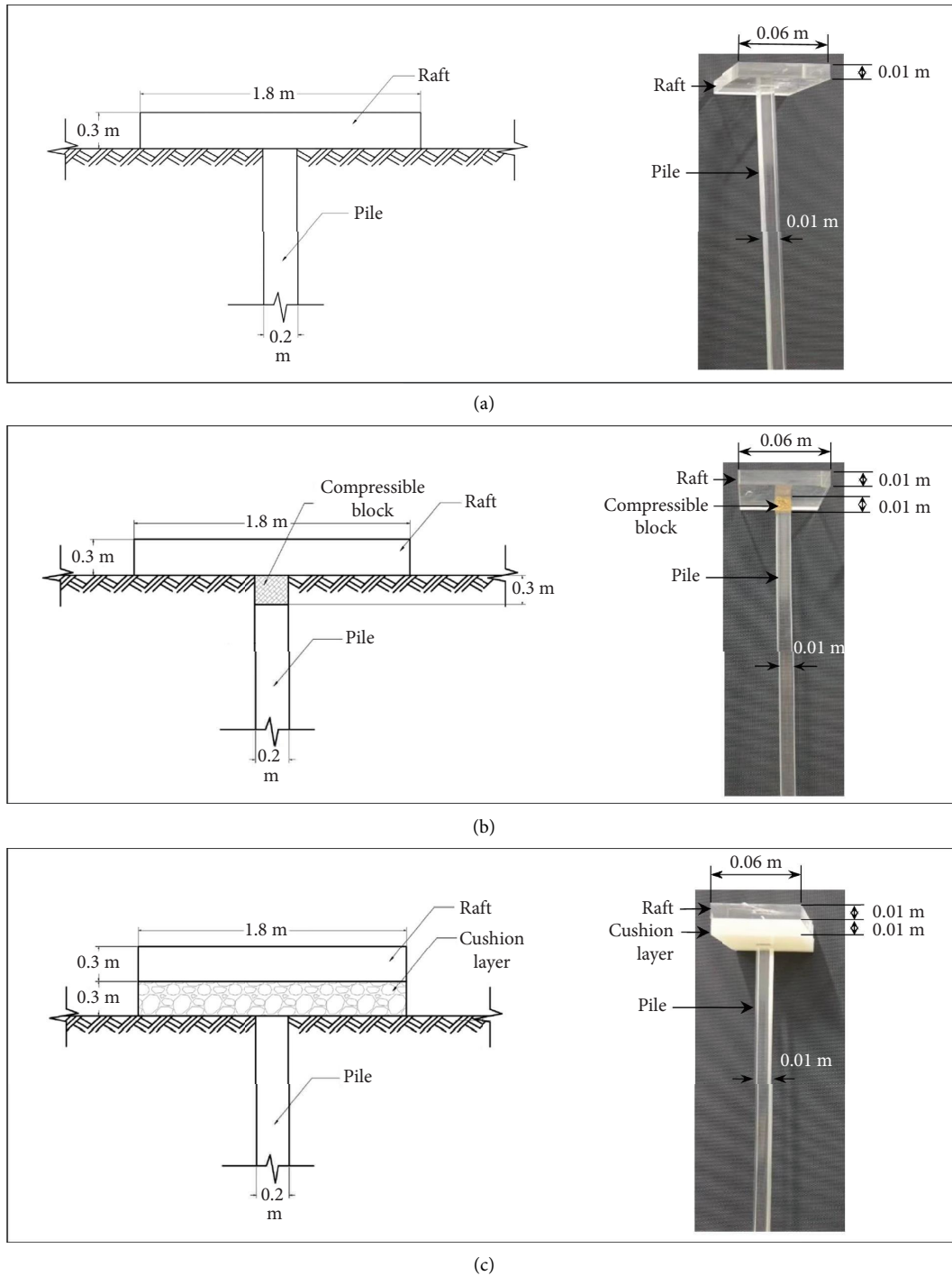
(a)

(b)

(c)

Figure 2: Schematic drawing of (a) PRF, (b) CBPRS, and (c) CLPRS.

different groups according to the test contents, as shown in Table 4.

3. Numerical Simulation

Based on the aforementioned experimental results, the finite element software ABAQUS was used to provide more insight into the dynamic load-bearing mechanism of the pile-raft systems.

3.1. Finite Element Modeling. First, a three-dimensional model was adopted in the Part module, including three types of pile-raft systems, as shown in Figure 4. The dimensions of the pile, raft, compressible block, and cushion layer were used as the prototypes, as shown in Table 2. The ground was generated with a size of $10 \times 10 \times 30$ m³. Then, the material and section properties were assigned to the elements of the pile-raft systems in the property module. An elastic, perfectly plastic model using the Mohr–Coulomb

TABLE 3: Properties of OMDS.

Property*	Value
Organic matter content, m (%)	5.32
Specific gravity, G_s	2.62
Water content, w (%)	12.23
Natural dry density, ρ_d (g/cm^3)	1.617
Minimum dry density, $\rho_{d\min}$ (g/cm^3)	1.570
Maximum dry density, $\rho_{d\max}$ (g/cm^3)	1.723
Cohesion, c (kPa)	4.2
Internal friction angle, φ (°)	22.23
Relative density, D_r	0.56
Poison ratio, υ	0.383

*The test type of soil property: m was acquired by the calcination method controlling 65°C of temperature, G_s acquired by the pycnometer method, w acquired by the drying method, ρ_d acquired by the ring knife method, $\rho_{d\min}$ acquired by the measuring cylinder method, $\rho_{d\max}$ acquired by the hammering method, c and φ acquired by the triaxial compression test. D_r was derived from ρ_d, $\rho_{d\min}$, and $\rho_{d\max}$; υ was derived from φ with their relationships to the static lateral pressure coefficient.
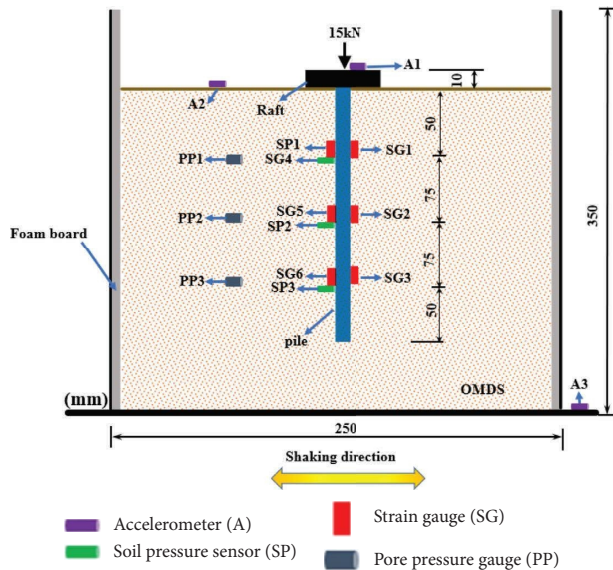

FIGURE 3: Placement of instruments.

failure criterion was adopted in this study with a non-associated flow rule. The calculation models for all scenarios in this section were implemented using the C3D8R element, an eight-node linear reduced integration solid element, available in the ABAQUS general-purpose finite element software. This element was capable of effectively simulating the 3D pile-soil model. The material properties of the soil, pile, raft, compressible block, and cushion layer are presented in Tables 2 and 3. Meanwhile, Rayleigh damping was used to describe the damping of all materials. Finally, each element of the model was meshed in the Mesh module. The elements on the contact surface had different material properties; hence, the soil closer to the pile was more densely divided to ensure the convergence of the calculation.

3.2. Numerical Modeling Procedure. The numerical modeling analysis had three steps: geostress equilibrium, vertical static load, and dynamic load. The vertical static load, a total of 450 kN, was applied to the center of the raft in five stages. The cyclic loading in the sinusoidal waveform was used on the bottom of the sand, which lasted 20 s.

The dynamic boundary condition adopted static-dynamic coupling boundary processing technology [28]. Specifically, the horizontal displacement along the side of the sand was released first during cyclic loading, and then the vertical displacement along the side of the sand was restrained. At the same time, the horizontal bearing reaction force under static load was applied. Finally, the preset time history of acceleration was introduced into the bottom of the sand to complete the static-dynamic coupling boundary.

4. Results and Interpretation

4.1. Acceleration. Figure 5 shows the test results of the time histories of accelerations for the three different connection forms of the pile-raft systems, and the calculated results are shown in Figure 6.

Because of the pile-soil-raft interaction, the accelerations recorded on the raft and sand differed from those input from the shaking table or the ground bottom of the numerical models. The amplification factor of acceleration was usually used to study this law. Equation (1) was used to normalize the peak acceleration, and the amplification factors at different positions were obtained, as shown in Table 5.

$$\lambda = \frac{x}{y}, \qquad (1)$$

where λ denotes the amplification factor of acceleration, x is the peak acceleration recorded on the accelerometer, and y is the peak acceleration input from the shaking table.

The peak acceleration measured on the top of the raft and the surface of the sand apparently exceeded the values input from the shaking table at the bottom under the three types of connection conditions, as shown in Figure 5. Table 5 shows that the amplification coefficients of the experimental results ranged from 1.5 to 2.8. These results were consistent with the previously reported findings of Zhang et al. [29] showing that soils could obviously amplify ground motions. Moreover, the peak soil and raft accelerations of CLPRS and CBPRS were found to be lower than those of PRF, implying that the disconnection between the pile and the raft could weaken the amplification effect of soil on acceleration. This was also reported by Ha et al. [30]. Importantly, the amplification factor on the top of the CBPRS raft was lower than that on the surface of sand, which was contrary to PRF [31]. In addition, the reduction in acceleration on the top of the raft weakened the inertial force of the superstructure caused by the horizontal cycle load. This meant that the compressible block played a significant isolation role under the test conditions in this study.

Table 5 also shows that the calculated peak acceleration amplification factors of the three types of pile-raft systems were consistent with those measured using the shaking table test. For example, compared with the results in PRF, the experimental and calculated peak accelerations of the raft top could be reduced by 42% and 45%, respectively, after the embedment of the compressible block, while the

TABLE 4: Test program.

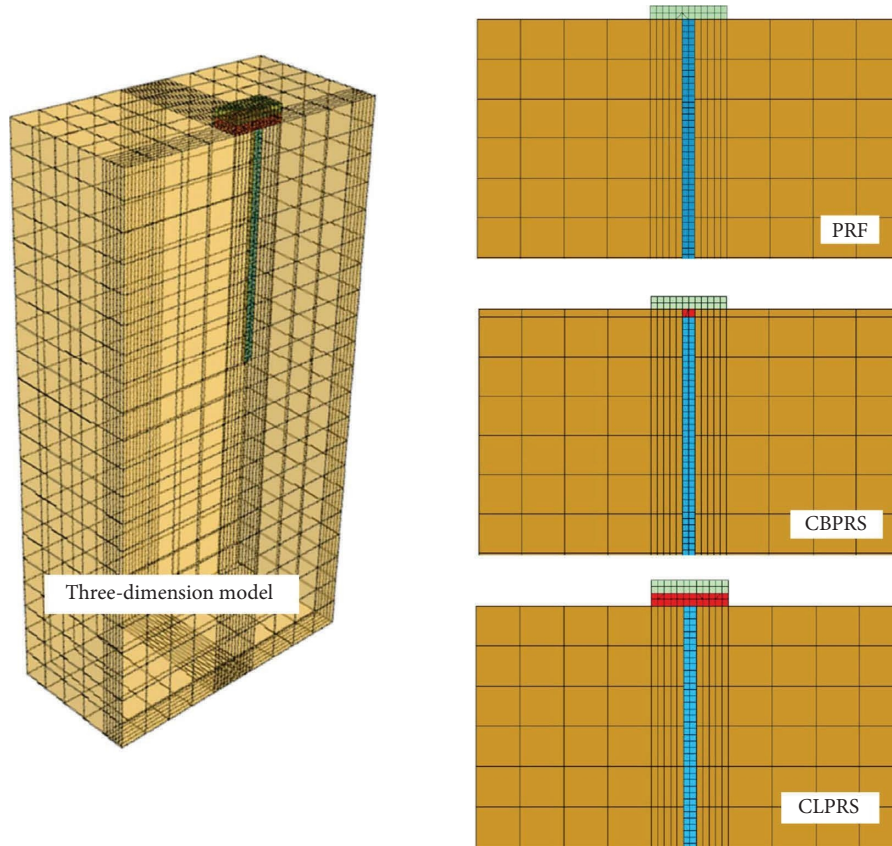| Connection mode	Acceleration, a_m	Waveform	Shaking frequency, f
PRF CBPRS CLPRS	$a_m = 6 \times 0.3\,g = 1.8\,g$	Sine wave	$S_f = \sqrt{S_a/S_l} = 13.416$ Hz

FIGURE 4: Finite element mesh of pile-raft systems.

experimental and calculated peak accelerations of the sand surface were reduced by 8% and 9%, respectively, after the embedment of the cushion layer. This verified the feasibility of numerical simulation in this study. This also implied that the isolation effect of the compressible block was relatively obvious.

The amplification factors of peak acceleration to reveal the acceleration response of the ground at different depths along the pile are shown in Figure 7. The amplification factors increased from bottom to top during sine wave transmission from the bottom of the site. Moreover, the amplification factors of CBPRS and CLPRS along the pile were lower than those of PRF. The reason was that the ground was obviously affected by the dynamic interaction of the larger stiffness with the connection of the pile and raft. When the pile top and raft were separated by a cushion layer or compressible block, the ground was less affected by the inertia effect and the acceleration response of the ground was also weakened [18, 32].

4.2. Bending Moment along the Pile.

The bending moments were calculated using equation (2) according to the pile flexural rigidity, and its measured strain value was derived from the strain gauge recorded along the instrumented pile, as shown in Figure 8.

$$M = \frac{(\varepsilon_1 - \varepsilon_2)\text{EI}}{b}, \qquad (2)$$

where M is the peak bending moment, ε_1 and ε_2 are tensile and compressive strains of each test section, respectively, E is Young's modulus of the model pile, I is the inertia moment of the pile section against the neutral axis, and b is the side length of the model pile.

The time history of the bending moment along the pile of the PRF was basically the same under cyclic loading conditions, showing sinusoidal regulation, as shown in Figures 8(a)–8(c). Figure 8(d) shows the peak bending moment along the pile of PRF. It was apparent that the bending moment closer to the pile top was greater than that
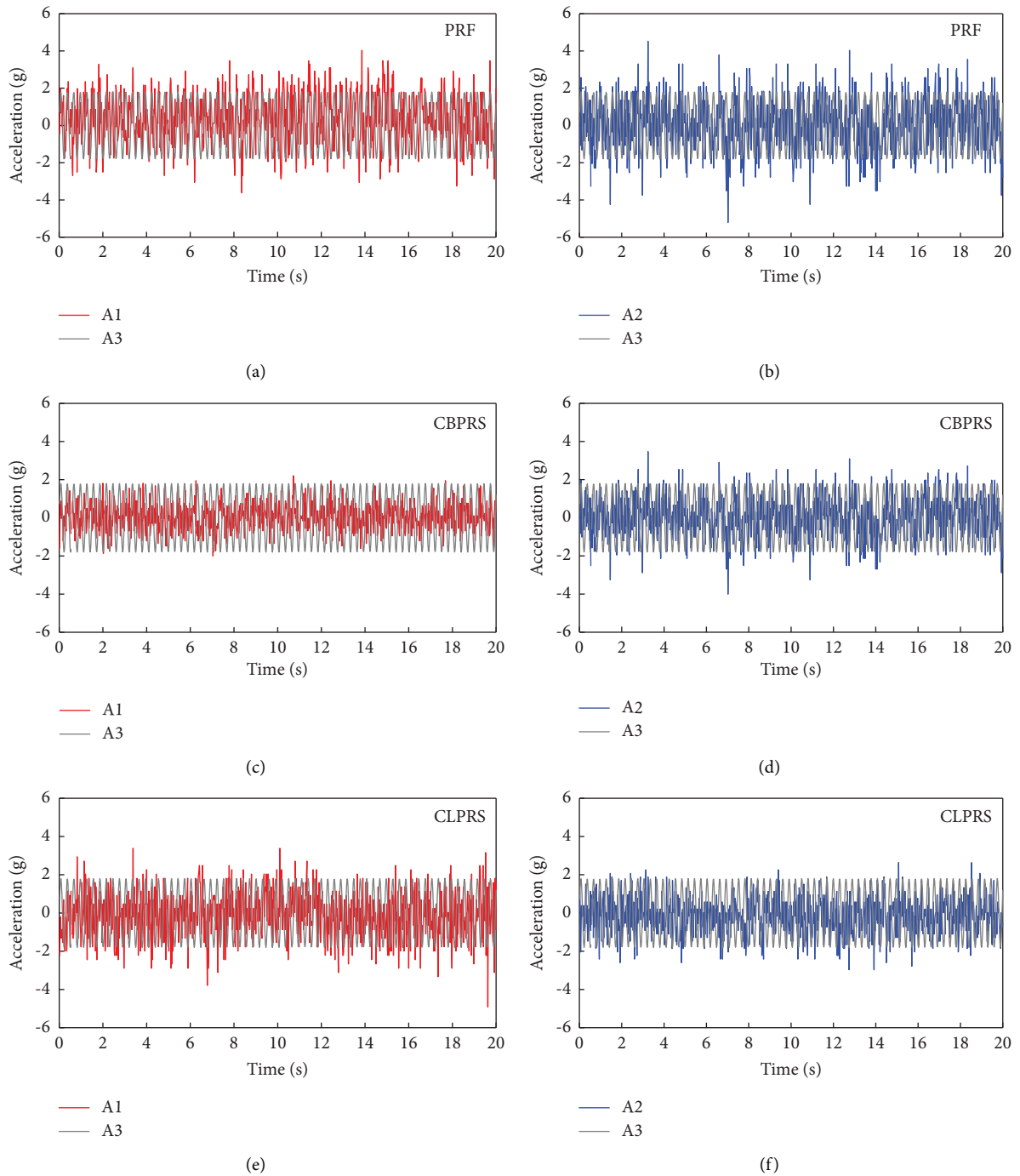
Figure 5: Time histories of acceleration acquired by tests (a) on the top of raft, PRF; (b) on the surface of sand, PRF; (c) on the top of raft, CBPRS; (d) on the surface of sand, CBPRS; (e) on the top of raft, CLPRS; and (f) on the surface of sand, CLPRS.

closer to the shaking table, consistent with the results of Banerjee et al. [33] and Wang et al. [34]. The peaks of the positive and negative bending moments were approximately symmetrically distributed along the pile.

Figure 9 shows the calculated peak bending moment along the pile in different connections. The maximum bending moment of the PRF was closer to the pile head and decreased gradually along the pile. This was consistent with the bending moment measured using the shaking table test,

as reported by this paper and Baziar et al. [35]. However, the bending moments of CBPRS and CLPRS were nearly equal to zero at the pile head; they first increased and then decreased along the pile, as reported by Kumar et al. Rasouli and Fatahi, and Ko et al. [18, 36, 37]. The maximum bending moments of CBPRS and CLPRS decreased by 71.7% and 46.8%, respectively, due to the separation of the pile and raft. These results showed that the flexure performance of the compressible block and cushion layer was better than that of
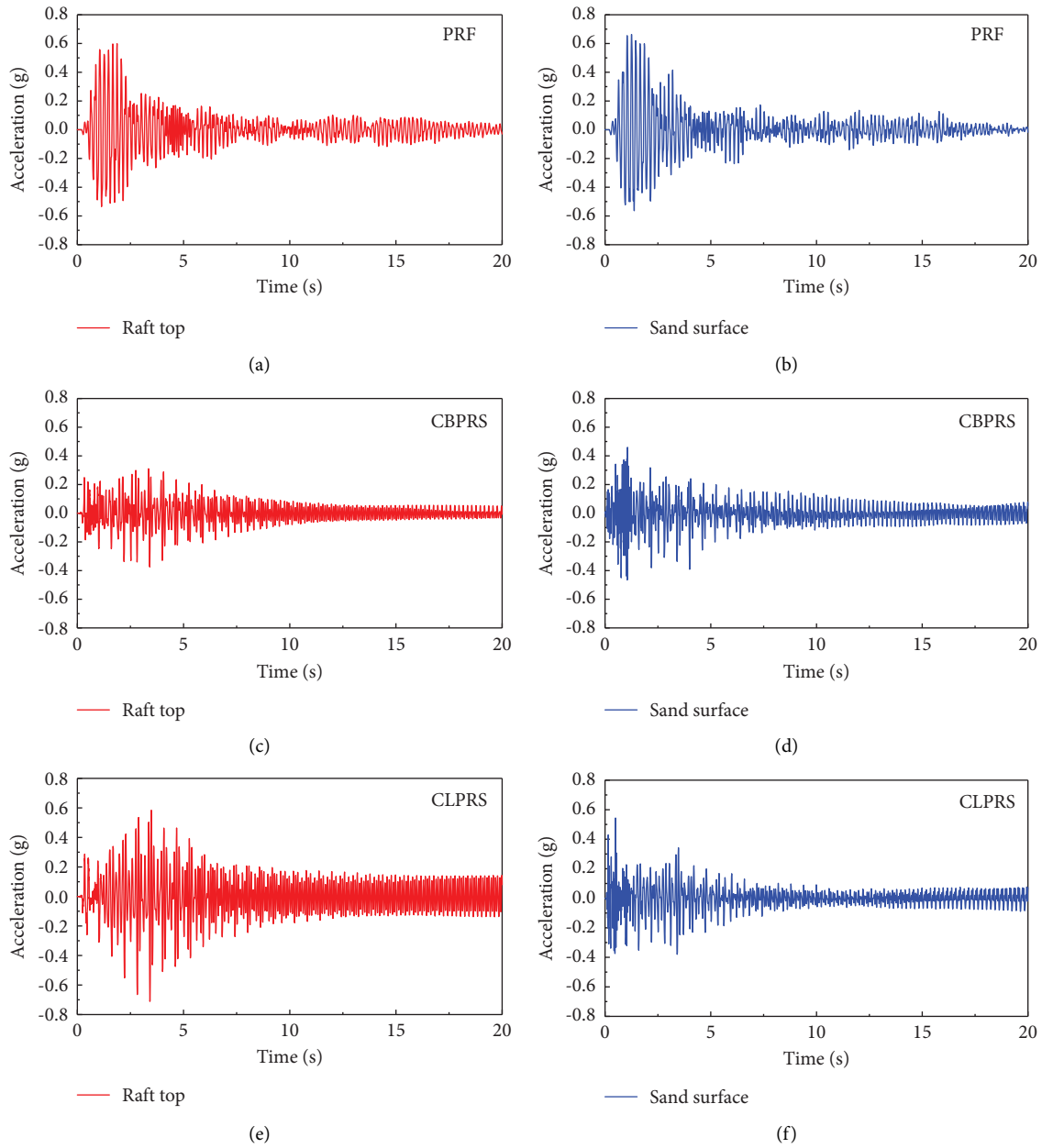
FIGURE 6: Time histories of acceleration acquired by numerical simulation (a) on the top of raft, PRF; (b) on the surface of sand, PRF; (c) on the top of raft, CBPRS; (d) on the surface of sand, CBPRS; (e) on the top of raft, CLPRS; and (f) on the surface of sand, CLPRS.

TABLE 5: The amplification factor of peak acceleration.

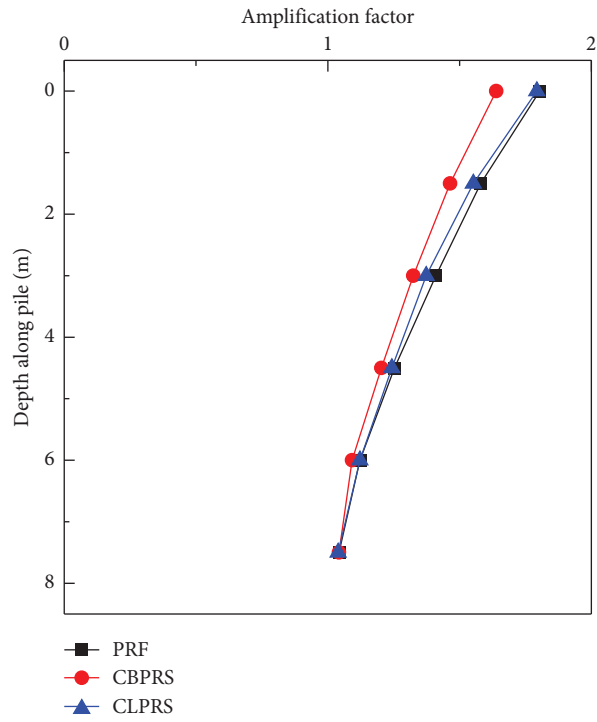| Case	y		Position	x		λ	
	Test (g)	Calculation (g)		Test (g)	Calculation (g)	Test	Calculation
PRF			Raft top	A1-4.896	0.623	2.719	2.077
			Soil surface	A2-4.278	0.613	2.380	2.043
CBPRS	A3-1.800	0.300	Raft top	A1-2.862	0.337	1.590	1.123
			Soil surface	A2-3.648	0.402	2.030	1.340
CLPRS			Raft top	A1-4.086	0.580	2.270	1.930
			Soil surface	A2-3.924	0.556	2.180	1.853

FIGURE 7: Calculated amplification factor of the peak acceleration along the pile.
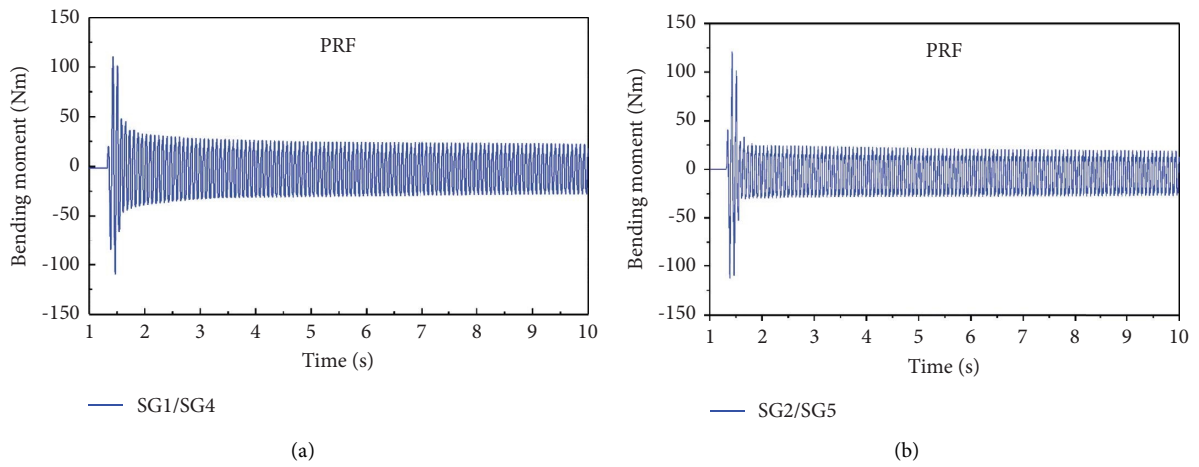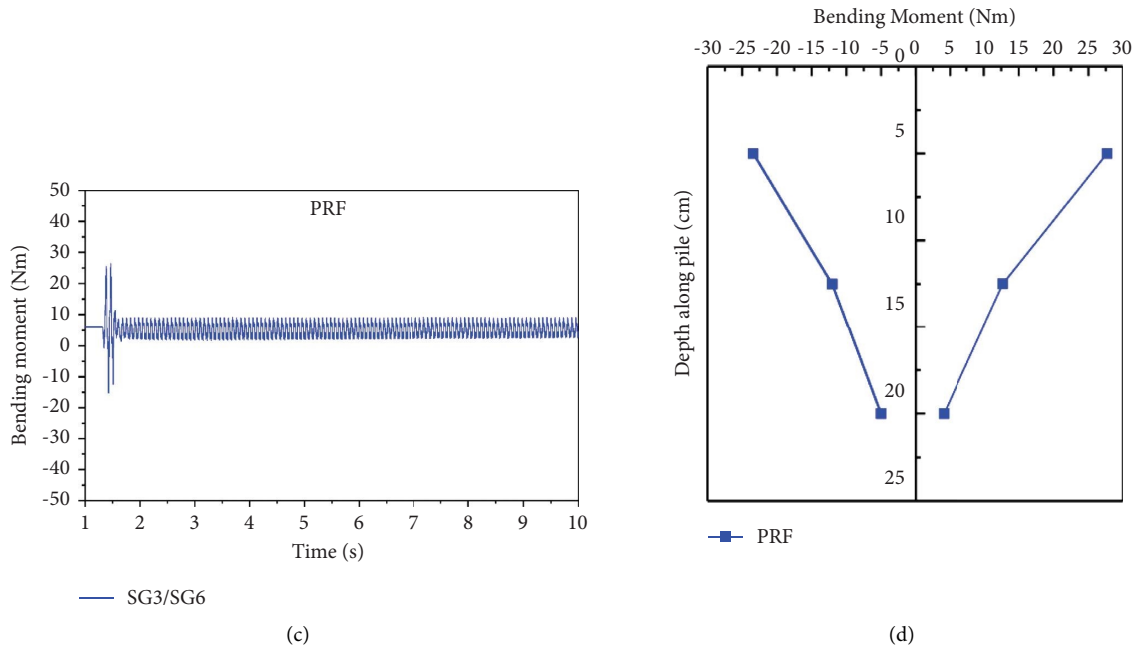

(a)

(b)

FIGURE 8: Continued.

(c)

(d)

FIGURE 8: Dynamic bending moment of PRF acquired by the following tests: (a) time history at 5 cm below the pile top; (b) time history at 12.5 cm below the pile top; (c) time history at 20 cm below the pile top; and (d) peak bending moment along the pile.
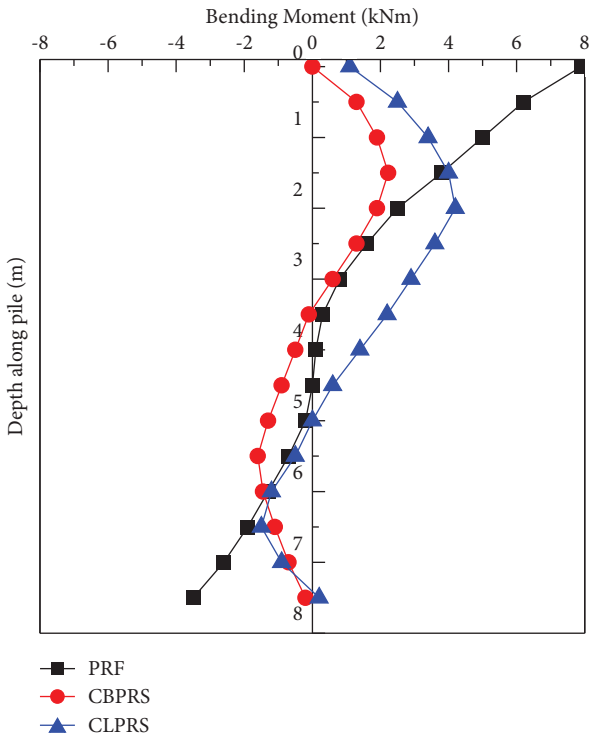

FIGURE 9: Peak bending moment along the pile acquired by numerical simulation.
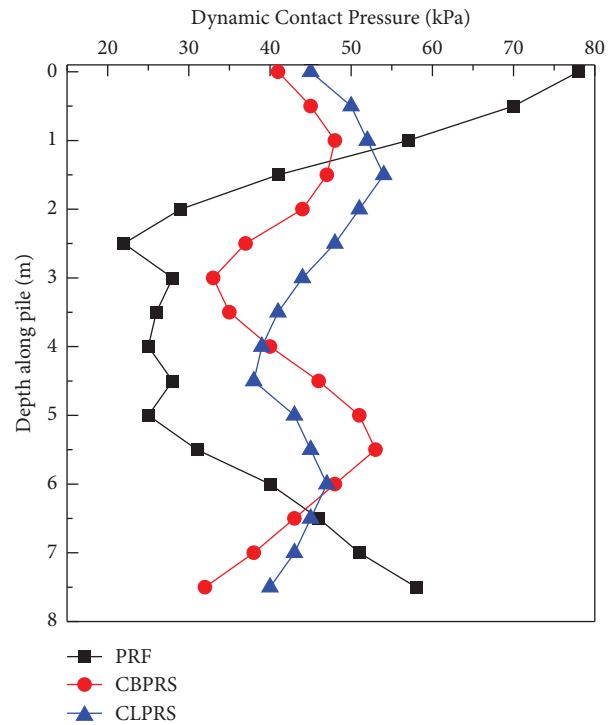

FIGURE 10: Peak contact pressure between pile and soil acquired by numerical simulation.

PRF, thus effectively avoiding the shear failure of the pile head. It was concluded that the compressible block performed better overall.

4.3. Computed Results of Dynamic Contact Pressure. The dynamic response of the pile-raft systems was affected by the dynamic interaction between the pile and soil [38]. Hence,

the dynamic contact pressure between the pile and soil was recorded, as shown in Figure 10. The distribution of the dynamic contact pressure of the PRF along the pile was K-shaped, which was consistent with the results of the shaking table test conducted by Qing et al. [39]. However, the dynamic contact pressures of CBPRS and CLPRS in the range of 30–50 kPa were distributed more evenly than those of PRF. This indicated that the bearing capacity of the soil around the pile was more uniformly mobilized when the pile and raft were disconnected, which was more beneficial to the use of pile strength. Meanwhile, the dynamic soil pressure at the pile head was reduced by approximately 50%, which could effectively avoid pile head failure.

5. Conclusions

This study mainly dealt with the aseismic performances of the three types of pile-raft systems under the cyclic loading of the horizontal sine wave. Overall, the systems with different connection forms showed certain variation rules and differences under cyclic loading. The following conclusions were drawn by comparing the model test and numerical simulation data.

(1) The disconnection between the pile and the raft could weaken the amplification effect of the raft top and soil surface on acceleration. The peak acceleration of the raft top could be reduced by more than 40%, after the embedment of the compressible block, while the peak acceleration of the soil surface could be reduced by 8%, after the embedment of the cushion layer.

(2) Due to the separation of the pile and raft, the maximum bending moments of the CBPRS and CLPRS decreased by 71.7% and 46.8%, respectively, effectively avoiding shear failure of the pile head.

(3) The embedment of the cushion layer and the compressible block could well mobilize the potential of the ground around the pile, which was more beneficial to the use of pile strength. Meanwhile, the dynamic soil pressure at the pile head was reduced by approximately 50%, which could effectively avoid pile head failure.

(4) The results of the shaking table test and numerical simulation showed that the dynamic response of the pile-raft systems was closely related to the elastic modulus of the connecting material between the pile and the raft. The acceleration amplification effect on the top of the raft decreased, and the peak bending moment at the pile head decreased with the decrease in the elastic modulus. Moreover, the distribution of the dynamic contact pressure between the pile and soil became more uniform. Therefore, the test condition of this paper indicated that the isolation effect of the compressible block was relatively obvious.

Data Availability

The data that support the findings of this study are available from the corresponding author upon reasonable request.

References

[1] H. Poulos, "Piled raft foundations: design and applications," *Géotechnique*, vol. 51, no. 2, pp. 95–113, 2001.

[2] X. Liu, R. Wang, and J.-M. Zhang, "Centrifuge shaking table tests on 4 × 4 pile groups in liquefiable ground," *Acta Geotechnica*, vol. 13, no. 6, pp. 1405–1418, 2018.

[3] P. Deb and S. Pal, "Nonlinear analysis of lateral load sharing response of piled raft subjected to combined V-L loading," *Marine Georesources and Geotechnology*, vol. 39, no. 8, pp. 994–1014, 2020.

[4] P. Deb and S. Pal, "Structural and geotechnical aspects of piled raft foundation through numerical analysis," *Marine Georesources and Geotechnology*, vol. 40, no. 7, pp. 823–846, 2021.

[5] H. S. Liu, "Earthquake damage and cause analysis of pile foundation-inspiration from Hanshin earthquake in Japan," *Earthquake Resistant Engineering*, 1999.

[6] K. Khalifa, M. Y. Fattah, and N. M. Salim, "The role of granular cushion in load sharing of unconnected piled rafts in clayey soils," *Engineering and Technology Journal*, vol. 39, no. 12, pp. 1789–1796, 2021.

[7] M. Y. Fattah, N. M. Salim, and K. R. Khalifa, "Parametric study of unconnected piled rafts in clayey soil using finite element method," *Innovative Infrastructure Solutions*, vol. 8, no. 1, p. 16, 2023.

[8] I. H. Wong, M. F. Chang, and X. D. Cao, *Raft Foundations with Disconnected Settlement-Reducing Piles*, ICE Publishing, London, UK, 2000.

[9] A. Lawal, *A Review of: Heat Exchanger Design*, Arthur P. Fraas John Wiley and Sons, New York, NY, USA, 2nd edition, 1989.

[10] T. Doi, Y. Murono, H. Iwai, and F. Zhang, "Numerical investigation of dynamic behavior of composite foundation composed of soilbags and piles by 3D elastoplastic FEM," *Soils and Foundations*, vol. 62, no. 3, Article ID 101158, 2022.

[11] X. D. Cao, I. H. Wong, and M.-F. Chang, "Behavior of model rafts resting on pile-reinforced sand," *Journal of Geotechnical and Geoenvironmental Engineering*, vol. 130, no. 2, pp. 129–138, 2004.

[12] F. Tradigo, F. Pisano, C. di Prisco, and A. Mussi, "Non-linear soil–structure interaction in disconnected piled raft foundations," *Computers and Geotechnics*, vol. 63, pp. 121–134, 2015.

[13] F.-Y. Liang, L.-Z. Chen, and X.-G. Shi, "Numerical analysis of composite piled raft with cushion subjected to vertical load," *Computers and Geotechnics*, vol. 30, no. 6, pp. 443–453, 2003.

[14] G. Zheng, X.-F. Gao, and Y.-H. Ren, "A study on the interaction of cap(foundation), pile and soil," *Chinese Journal of Geotechnical Engineering*, vol. 26, no. 3, pp. 307–312, 2004.

[15] G. Zheng, D. L. Liu, and J. X. Li, "Experimental study on behaviors of piled foundation with connected and

disconnected piles," *Yantu Gongcheng Xuebao/chinese Journal of Geotechnical Engineering*, vol. 31, no. 1, pp. 89–94, 2009.

[16] H. G. Poulos, "Use of stiffness inserts in pile groups and piled rafts," *Proceedings of the Institution of Civil Engineers- Geotechnical Engineering*, vol. 159, no. 3, pp. 153–160, 2006.

[17] Z. Gang, "Mechanism of settlement control of piled raft with gap or compressible block at pile top for support of railway embankment," *China Civil Engineering Journal*, vol. 42, no. 5, pp. 125–132, 2009.

[18] A. Kumar, D. Choudhury, and R. Katzenbach, "Effect of earthquake on combined pile-raft foundation," *International Journal of Geomechanics*, vol. 16, no. 5, 2016.

[19] V. F. Fioravante and D. G. Giretti, "Contact versus noncontact piled raft foundations," *Canadian Geotechnical Journal*, vol. 47, no. 11, pp. 1271–1287, 2010.

[20] A. S. Azizkandi, M. H. Baziar, and A. F. Yeznabad, "3D dynamic finite element analyses and 1 g shaking table tests on seismic performance of connected and nonconnected piled raft foundations," *KSCE Journal of Civil Engineering*, vol. 22, no. 5, pp. 1750–1762, 2017.

[21] A. S. Azizkandi, M. Aghamolaei, and S. H. Hasanaklou, "Evaluation of dynamic response of connected and nonconnected piled raft systems using shaking table tests," *Soil Dynamics and Earthquake Engineering*, vol. 139, Article ID 106366, 2020.

[22] X. Han, Y. Li, J. Ji, J. Ying, W. Li, and B. Dai, "Numerical simulation on the seismic absorption effect of the cushion in rigid-pile composite foundation," *Earthquake Engineering and Engineering Vibration*, vol. 15, no. 2, pp. 369–378, 2016.

[23] D. Y. Li and B. M. Wang, *Model Test of Structure*, Science Press, Beijing, China, 1996.

[24] J. C. Hu, D. H. Bai, W. H. Wang, Z. Lin, X. Xiang, and L. Wang, "Deep electrical anomaly in the M7.5 Qiongzhou earthquake region and its relation with future seismicity," *Acta Seismologica Sinica (English edition)*, vol. 20, no. 3, pp. 273–279, 2007.

[25] J. Du, G. Zheng, B. Liu, N. J. Jiang, and J. Hu, "Triaxial behavior of cement stabilized organic-matter-disseminated sand," *Acta Geotechnica*, vol. 16, no. 1, pp. 211–220, 2021.

[26] *Standard for Geotechnical Testing Method*, China Planning Press, Beijing, China, 2019.

[27] Z. G. Tang, Y. Z. Wang, and X. F. Duan, "Development and performance evaluation of separable high-frequency response miniature pore water pressure transducer," *Chinese Journal of Geotechnical Engineering*, vol. 43, no. 7, pp. 1210–1219, 2021.

[28] R. Wang, H. Y. Zhuang, and G. X. Chen, "Seismic response of subway underground station buried in liquefiable soil foundation with the ground surface slight inclined," *Earthquake Engineering and Engineering Dynamics*, 2018.

[29] L. Zhang, S. H. Goh, and J. Yi, "A centrifuge study of the seismic response of pile-raft systems embedded in soft clay," *Géotechnique*, vol. 67, no. 6, pp. 479–490, 2017.

[30] J.-G. Ha, K.-W. Ko, S.-B. Jo, H. J. Park, and D. S. Kim, "Investigation of seismic performances of unconnected pile foundations using dynamic centrifuge tests," *Bulletin of Earthquake Engineering*, vol. 17, no. 5, pp. 2433–2458, 2018.

[31] M. Y. Fattah, H. H. Karim, and M. K. M. Al-Recaby, "Investigation of the end bearing load in pile group model in dry soil under horizontal excitation," *Acta Geotechnica Slovenica*, vol. 18, pp. 79–106, 2021.

[32] M. Baziar, F. Rafiee, C.-J. Lee, and A. Saeedi Azizkandi, "Effect of superstructure on the dynamic response of nonconnected piled raft foundation using centrifuge modeling," *International Journal of Geomechanics*, vol. 18, no. 10, 2018.

[33] S. Banerjee, S. H. Goh, and F. H. Lee, "Earthquake-induced bending moment in fixed-head piles in soft clay," *Géotechnique*, vol. 64, no. 6, pp. 431–446, 2014.

[34] R. Wang, X. Liu, and J.-M. Zhang, "Numerical analysis of the seismic inertial and kinematic effects on pile bending moment in liquefiable soils," *Acta Geotechnica*, vol. 12, no. 4, pp. 773–791, 2017.

[35] M. Baziar, F. Rafiee, A. Saeedi Azizkandi, and C. J. Lee, "Effect of super-structure frequency on the seismic behavior of pile-raft foundation using physical modeling," *Soil Dynamics and Earthquake Engineering*, vol. 104, pp. 196–209, 2018.

[36] H. Rasouli and B. Fatahi, "A novel cushioned piled raft foundation to protect buildings subjected to normal fault rupture," *Computers and Geotechnics*, vol. 106, pp. 228–248, 2019.

[37] K. W. Ko, H. J. Park, J. G. Ha et al., "Evaluation of dynamic bending moment of disconnected piled raft via centrifuge tests," *Canadian Geotechnical Journal*, vol. 56, no. 12, pp. 1917–1928, 2019.

[38] P. Li, J. Yang, and Z. Lu, "Shaking table test and theoretical analysis of the pile-soil-structure interaction at a liquefiable site," *The Structural Design of Tall and Special Buildings*, vol. 27, no. 15, 2018.

[39] Y. Q. Chen, X. L. Lu, P. Z. Li, and J. G. Hou, "Dynamic response of piles in SSI system with various soils," *Engineering Journal of Wuhan University*, vol. 38, no. 4, pp. 50–54, 2005.